



Effects of various light-intensity and temperature environments on the photovoltaic performance of dye-sensitized solar cells

Ji Hoon Kim^a, Kook Joo Moon^b, Jong Man Kim^{a,b,c}, Dongyun Lee^{a,b,c},
Soo Hyung Kim^{a,b,c,*}

^a Department of Nano Fusion Technology and BK21 Plus Nano Convergence Technology Division, Pusan National University, 30 Jangjeon-dong, Geumjung-gu, 609-736 Busan, Republic of Korea

^b Samsung Advanced Circuit Engineering, Pusan National University, 30 Jangjeon-dong, Geumjung-gu, 609-736 Busan, Republic of Korea

^c Department of Nano Energy Engineering, Pusan National University, 30 Jangjeon-dong, Geumjung-gu, 609-736 Busan, Republic of Korea

Received 21 October 2014; received in revised form 24 December 2014; accepted 9 January 2015

Communicated by: Associate Editor Frank Nüesch

Abstract

Low-cost dye-sensitized solar cells (DSSCs), which offer a clean and renewable energy source, have attracted considerable attention. However, cell efficiency and performance stability remains a primary concern. The photovoltaic performance of DSSCs is significantly affected by both light intensity and operating temperature. In order to maintain the optimum operating conditions for DSSCs in practical application environments, it is important to understand the combinational effects of light intensity and operating temperature on their characteristic behaviors. In this work, we systematically investigate the conditions for satisfactory photovoltaic performance of DSSCs in various light-intensity and temperature environments. At light intensities lower than 1-Sun condition (i.e. $<100 \text{ mW cm}^{-2}$), the power conversion efficiency (PCE) of DSSCs is significantly decreased with increasing operating temperature due to the enhanced charge recombination rate resulting from the lowered viscosity of the liquid electrolyte. However, at light intensities higher than the 1-Sun condition (i.e. $>100 \text{ mW cm}^{-2}$), the PCE of DSSCs is stably maintained at elevated temperatures ranging from -4 to $60 \text{ }^\circ\text{C}$ due to the increased concentration of photogenerated electrons, which compensate for the loss of electrons by charge recombination between photogenerated electrons and liquid electrolyte ions.

© 2015 Elsevier Ltd. All rights reserved.

Keywords: Light intensity; Temperature; Dye-sensitized solar cell; Charge transfer kinetics

1. Introduction

Solar cells have attracted considerable attention as clean and renewable energy sources that can form an alternative to power generation from fossil fuels and hydroelectric

systems. However, their performance is constrained by weather conditions such as ambient temperature and incident light intensity. In the backdrop of studying the feasibility of practically utilizing solar cells to harness energy in the light of prevailing weather conditions, according to the annual Korean weather forecast report, the monthly average light intensity and monthly average air temperature of three major cities (Seoul [$37^\circ30'N$, $127^\circ07'E$], Busan [$35^\circ06'N$, $129^\circ03'E$], and Jeju island [$33^\circ31'N$, $126^\circ32'E$]) in Korea lie in the ranges of 0.3–1 Sun and -4 to $35 \text{ }^\circ\text{C}$, respectively, as shown in Fig. 1 (The National Weather

* Corresponding author at: Department of Nano Fusion Technology and BK21 Plus Nano Convergence Technology Division, Pusan National University, 30 Jangjeon-dong, Geumjung-gu, 609-736 Busan, Republic of Korea. Tel.: +82 51 9307737; fax: +82 51 5142358.

E-mail address: sookim@pusan.ac.kr (S.H. Kim).

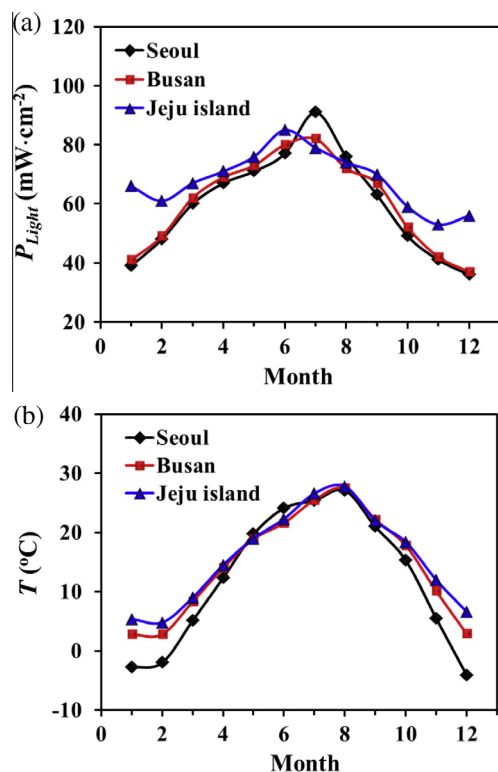


Fig. 1. Monthly variation in (a) light intensity conditions (P_{Light}) and (b) air temperature (T) of three major cities in the Republic of Korea (i.e. Seoul [37°30'N, 127°07'E], Busan [35°06'N, 129°03'E], and Jeju island [33°31'N, 126°32'E]).

Service, Solar energy resource distribution map, 2012). Various natural factors such as seasonal changes, sunlight irradiation, and locally windy and cloudy conditions create the appreciable differences in light intensity and cell temperature, and therefore, the resulting photovoltaic performance of dye-sensitized solar cells (DSSCs) installed in a given area can significantly vary (Tripathi et al., 2014; Kim and Kim, 2012; Raga and Fabregat-Santiago, 2012; Gonzalez-Valls et al., 2011; Barnes et al., 2011; Lee et al., 2010; Akira, 2009; Berginc et al., 2008, 2007; Ocakoglu et al., 2008; O'Regan and Durrant, 2006; Lagemaat and Frank, 2001). Furthermore, the addition of supplementary equipment to DSSCs e.g. solar concentrators (Moon et al., 2013; Choi et al., 2011; Zhang et al., 2008; Mittelman et al., 2007), heat exchangers (Kong et al., 2014; He et al., 2006; Tripanagnostopoulos et al., 2002), and surface cleaning systems (Ahn et al., 2013c; Park et al., 2011; Faustini et al., 2010; Zhu et al., 2010; Min et al., 2008) can strongly influence the photovoltaic properties of DSSCs by affecting the light intensity and operating temperature, which mostly perturbs the electron generation in the photoelectrode and the charge transport in the liquid electrolyte. However, numerous previous studies on DSSCs have been conducted under the standard 1-Sun condition (i.e. 100 mW cm⁻²) at room temperature during their characterization (Park et al., 2013; Ahn et al., 2012, 2013a,b; Muduli et al., 2012; Koo et al., 2008; Mor et al., 2006). Therefore, the

basic understanding of the functioning and practical applications of DSSCs can be limited due to the lack of useful data pertaining to DSSCs tested under various light intensities and operating temperature conditions.

In this study, we systematically investigated the effects of both light intensity and operating temperature on the photovoltaic performance of DSSCs. Detailed analyses were carried out to examine the variations in electron transport in the liquid electrolyte, and the proof-of-concept is also provided to explain the changes in the power conversion efficiency (PCE) of DSSCs. In particular, we varied the light intensity by using light filters to achieve intensities lower than 1 Sun-condition (e.g. 25 and 50 mW cm⁻²) and convex-lens-assisted solar concentrators for intensities greater than the 1-Sun condition (e.g. 267 and 570 mW cm⁻²). The operating temperature of the DSSCs was also controlled in the range from -4 to 60 °C using a Peltier cell.

2. Experimental

2.1. Materials and solar cell preparation

Commercially available TiO₂ paste (T/SP, Solaronix, Zollikon, Switzerland) was used without further treatment as the high-surface-area porous electron-transferring material (Zhu et al., 2011; Li et al., 2010; Kim et al., 2010; Calogero and Marco, 2008; Hore et al., 2006). As the photoelectrode layer, a TiO₂ nanoparticle (NP)-accumulated thin layer was applied via a screen-printing process on a fluorine-doped tin oxide (FTO) glass (SnO₂:F, 7 Ω sq⁻¹, Pilkington, Boston, USA) with a photoactive area of 0.6 cm × 0.6 cm. The FTO glass was thermally treated at 500 °C for 30 min after pretreatment with a solution of 0.247 mL of TiOCl₂ and 20 mL of deionized water to enhance the adhesion between the TiO₂ NP layer and the FTO glass. The resulting TiO₂ NP-accumulated layer formed on the FTO glass via screen-printing process was subsequently sintered in an electric furnace at 500 °C for 30 min and immersed in anhydrous ethanol containing 0.3 mM of Ru dye (Bu₄N)₂[Ru(Hdcbpy)₂(NCS)₂] (N719 dye, Solaronix, Zollikon, Switzerland) for 24 h at room temperature in order to allow the dye molecules to attach themselves to the entire surface of the TiO₂ NPs. The dye-soaked TiO₂-NP-based photoelectrode was subsequently rinsed with ethanol and dried in a convection oven at 80 °C for 10 min. As a counter electrode, we prepared Pt-coated FTO glass using an ion sputter (Model No. E1010, Hitachi, Chiyoda-ku, Japan) operated at 2.5 kV. Both the dye-soaked TiO₂ NP-based photoelectrode and the Pt-coated counter electrode were sealed together with a hot-melt polymer film (60-μm thick, Surllyn, DuPont, Wilmington, Delaware, USA) that was inserted between the two electrodes, and an iodide-based liquid electrolyte (AN-50, Solaronix) which has a 50 mM of iodide concentration in acetonitrile solvent and a small amount of additives including ionic liquid, lithium salt and pyridine

derivatives was subsequently injected into the interspace between the electrodes.

2.2. DSSC characterization

The light intensity was controlled by placing neutral density (ND) filters and a condenser lens in the illumination path. The condenser-lens-based solar concentrator employed in this study had a diameter of 30 mm, a center thickness of 2 mm, an edge thickness of 1.46 mm, and an effective focal length of 30 mm. The condenser lens was supported by a homemade vertical holder, and the focal length was varied by adjusting the rotating gauge (see Fig. 2, Choi et al., 2011). The operating temperature of the DSSCs was controlled using a Peltier cell (9501, Ferrotec Co., Ltd., Korea) in the temperature range from -4 to 60 °C. We measured the temperature of top and bottom sides of DSSCs by using a thermocouple. Here, the top side

of DSSCs was exposed to the external air and the bottom side of DSSCs was directly contacted with Peltier cell, respectively (Gonzalez-Valls et al., 2011; Halme et al., 2006). And the operating temperature was calculated by taking a mean value of top and bottom side temperature of DSSCs. The current density–voltage (J – V) characteristics of the resulting DSSCs fabricated in this study were measured under AM 1.5 simulated illumination with intensities ranging from 25 to 570 mW cm^{-2} (PEC-L11, Peccell Technologies, Inc., Yokohama, Kanagawa, Japan). The intensity of sunlight illumination was calibrated using a standard Si photodiode detector with a KG-5 filter. The J – V curves were automatically recorded using a Keithley SMU 2400 source meter (Cleveland, OH, USA) by illuminating the DSSCs. Electrochemical impedance spectroscopy (EIS) measurements of DSSCs were performed using an impedance analyzer (Ivium CompactStat, Ivium technologies, Netherlands). Bias potentials were set at the open-circuit voltage of the DSSCs under illumination from 25 to 570 mW cm^{-2} . 10 mV AC perturbation was applied at frequencies ranging from 0.1 Hz to 100 kHz. The impedance spectra were then analyzed by an equivalent circuit model interpreting the characteristics of the DSSCs. Briefly, the value of R_{fto} , R_i , R_{pt} were extracted from the start point, the width of third semicircle and first semicircle in the Nyquist plots, respectively. The viscosity of the liquid electrolyte was measured by a viscometer (6V-10, Brookfield Engineering Lab., MA, USA) by varying the temperature in the range from -5 to 50 °C.

3. Results and discussion

In order to examine the effect of operating temperature on the photovoltaic performance of the DSSCs, we varied the operating temperature of the DSSCs using a Peltier cell under the fixed 1-Sun irradiance condition (i.e. AM 1.5 & 100 mW cm^{-2}). From the values listed in Table 1 and Fig. 3a, we can clearly observe that the short-circuit current density (J_{sc}) and open-circuit voltage (V_{oc}) decrease with an increase in cell temperature. Both the J_{sc} and V_{oc} values of the DSSCs decrease from 14.78 mA cm^{-2} and 0.75 V at $T = -4$ °C to 13.56 mA cm^{-2} and 0.64 V at $T = 60$ °C, respectively, thereby resulting in a considerable reduction in the corresponding PCE value from 7.25% at $T = -4$ °C to 5.67% at $T = 60$ °C, respectively.

In order to determine the possible reasons for these observed phenomena, we performed an electrochemical impedance spectroscopy (EIS) measurement for the DSSCs operated at different temperatures. Further, from Table 1 and Fig. 3b, we note that the calculated electron lifetime ($\tau_e = [2\pi f_{\max}]^{-1}$, where f_{\max} denotes the maximum frequency) slightly reduces with increasing operating temperature, thereby suggesting that the photogenerated electrons diffuse further at lower temperatures. From the Nyquist plots (Fig. 3c) and the corresponding analyzed elemental resistance (Fig. 3d), we observe that the charge transfer resistance gradually reduces with increasing operating tem-

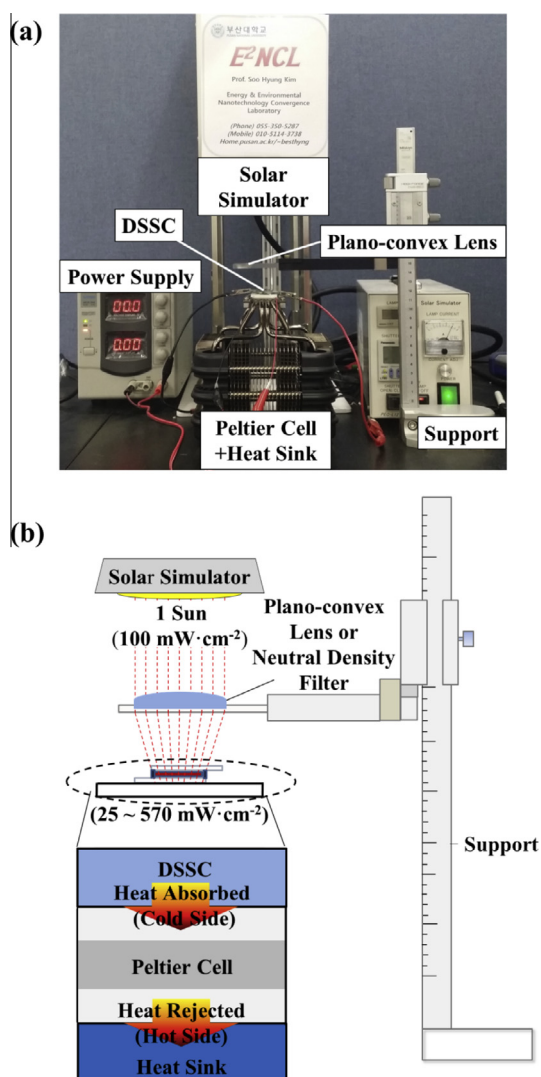


Fig. 2. (a) Photograph and (b) schematic of light intensity and operating temperature control systems for DSSC units.

Table 1

Summary of photovoltaic performance parameters of DSSCs operated at various temperatures under the fixed 1-Sun condition ($=100 \text{ mW cm}^{-2}$).

Temperature ($^{\circ}\text{C}$)	J_{sc} (mA cm^{-2})	V_{oc} (V)	FF	PCE (%)	R_s (Ω)	τ_e (ms)
-4	14.78	0.75	0.66	7.25	12.4	5.0
4	14.72	0.74	0.66	7.21	12.0	4.9
12	14.67	0.73	0.66	7.07	11.4	4.8
20	14.47	0.72	0.66	6.91	10.9	4.7
28	14.36	0.71	0.66	6.71	10.6	4.5
36	14.17	0.69	0.66	6.48	10.0	4.4
44	13.92	0.67	0.66	6.09	9.4	4.3
52	13.69	0.65	0.66	5.87	9.1	4.1
60	13.56	0.64	0.65	5.67	8.6	4.0

Note: J_{sc} : short circuit current, V_{oc} : open circuit voltage, FF: fill factor, PCE: power conversion efficiency, R_s : series resistance, τ_e : electron life time.

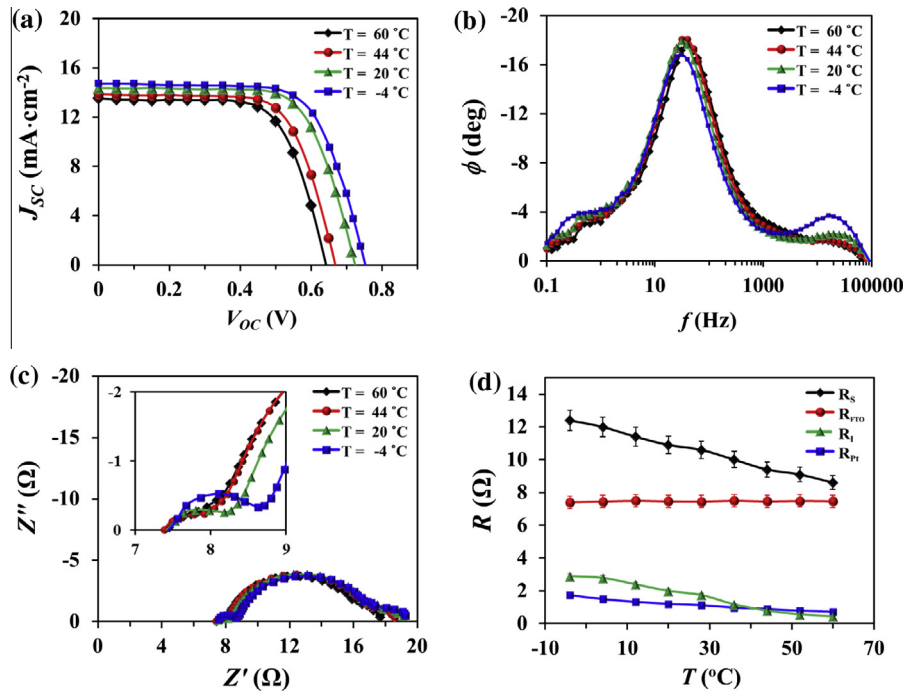


Fig. 3. (a) J - V curves, (b) Bode plots, (c) Nyquist plots, and (d) charge transfer resistance analysis of DSSCs operated at various temperatures under the fixed 1-Sun condition ($=100 \text{ mW cm}^{-2}$).

perature. In general, the total series resistance (R_S) of a DSSC can be represented as the expression $R_S = R_{FTO} + R_{Pt} + R_I$. Here, R_{FTO} denotes the resistance of the FTO-coated glass substrate, R_{Pt} the charge transfer resistance at the Pt-coated counter electrode, and R_I the diffusion resistance resulting from the transport of holes in the iodide-based liquid electrolyte. In our trials, there was no appreciable change in R_{FTO} at various cell temperatures. This suggests that cell temperature hardly affects the R_{FTO} values. However, both R_{Pt} and R_I gradually decrease with increasing operating temperature, thereby suggesting that the operating temperature strongly affects the charge transfer kinetics between the counter electrode and liquid electrolyte. We believe that the increase in cell temperature correspondingly changes the viscosity of the liquid electrolyte such that the charge recombination rate between photogenerated electrons and liquid electrolyte is accordingly affected.

The above speculation can be corroborated by directly measuring the viscosity of the liquid electrolyte as a function of temperature. From the results shown in Fig. 4, we note that the viscosity of liquid electrolyte linearly decreases with increasing operating temperature, thereby implying that the enhancement of ion mobility in the liquid electrolyte at high temperatures increases the charge recombination rate. As a result of the enhanced charge recombination rate at high temperatures, the average electron lifetime accordingly decreases. Therefore, the acceleration of charge transfer kinetics with increasing operating temperature results in reductions in both J_{sc} and V_{oc} values. As a proof-of-concept, a motor fan connected to a DSSC was employed to visualize the effect of operating temperature on the photovoltaic performance of DSSCs. Under the fixed 5.7-Sun condition (i.e. 570 mW cm^{-2}), a DSSC was operated at different temperature conditions ranging from -4 to 50 $^{\circ}\text{C}$. The motor fan exhibited very

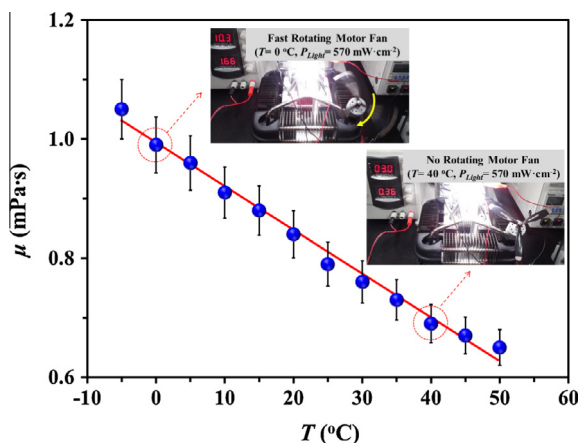


Fig. 4. The evolution of liquid electrolyte viscosity as a function of temperature (insets show the snapshots of a motor fan connected to a DSSC operated at 0 °C & 570 mW cm⁻² (upper image) and 40 °C & 570 mW cm⁻² (lower image)).

high rotation speeds over the temperature range from -4 to 40 °C, while it suddenly stopped rotating at temperatures greater than 40 °C, thereby suggesting that the current and voltage outputs from the DSSC significantly decrease due to the increased loss in photogenerated electrons resulting from enhanced charge transfer kinetics at higher operating temperatures.

Since the intensity of irradiated light on solar cells is directly related to variation in the cell temperature, we also examined the effects of light intensity in conjunction with operating temperature on the photovoltaic performance

of DSSCs. From Fig. 5a, we note that the J_{sc} values exhibit a significant increase with increase in the light intensity. However, no appreciable change in J_{sc} values for different operating temperatures is observed at a given light intensity. This is because of the increase in power input caused by higher light concentration. From Fig. 5b, we note that the V_{oc} value logarithmically increases with increasing light intensity. The V_{oc} value relatively steeply increases for low illumination conditions (i.e. ≤ 100 mW cm⁻²), and subsequently, it gradually increases with increasing light intensity for values greater than 100 mW cm⁻². In general, V_{oc} is proportional to the temperature, while the enhanced charge recombination rate resulting from the reduction in liquid electrolyte viscosity leads to a significant decrease in V_{oc} due to increase in the I_o value, as can be inferred from Eq. (1). The net result of these two contrasting effects eventually leads to a significant decrease in V_{oc} values at elevated temperatures, as shown in Fig. 5b. The expression for V_{oc} is given as

$$V_{oc} \approx \frac{nkT}{q} \ln \left(\frac{I_{sc}(X)}{I_o} \right) \quad (1)$$

Here n denotes the diode quality factor, k the Boltzmann constant, T the absolute temperature, q the electronic charge, X the light intensity, $I_{sc}(X)$ the short circuit current in light intensity of X , and I_o the reverse saturation current.

Fig. 5c shows the variation in the fill factor (FF) values as a function of light intensity. We note that the FF values significantly decrease with increasing light intensity at all operating temperatures. The reduction in FF values at high light intensities appears to occur due to the enhanced

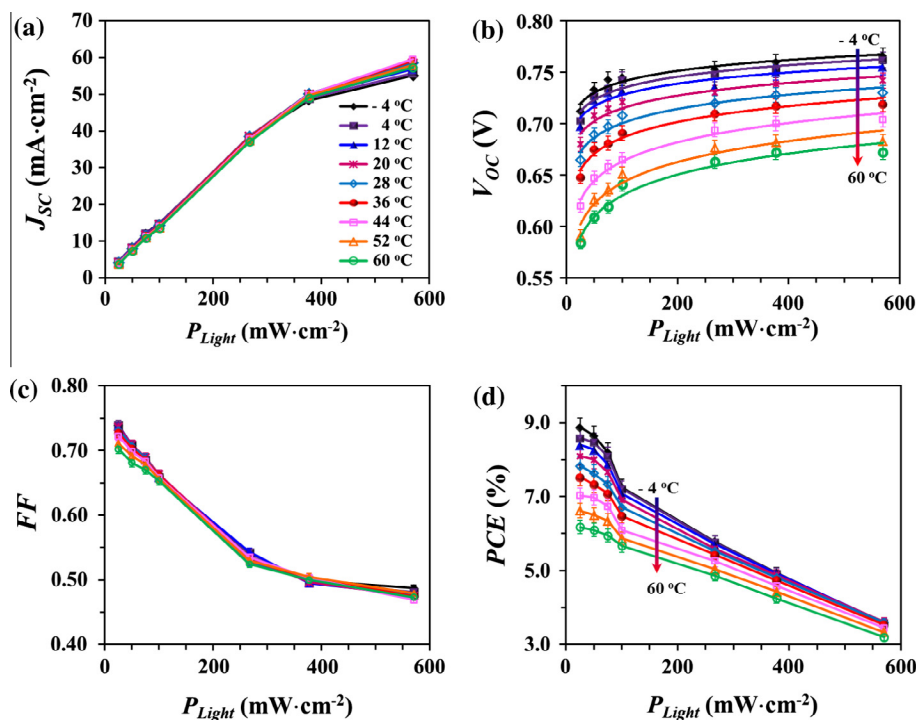


Fig. 5. (a) J_{sc} , (b) V_{oc} , (c) FF, and (d) PCE values of DSSCs operated at various temperatures and light intensities.

charge recombination rate due to the increased concentration of photogenerated electrons. It is interesting to note that the FF values are similar for each temperature even though they can be decreased at higher cell temperatures by the enhanced charge recombination rate due to reduction in liquid electrolyte viscosity. This is because the series resistance simultaneously decreases with increasing temperature; consequently, these two contrasting effects can lead to similar FF values at different operating temperatures. The PCE of DSSCs is observed to steeply decrease with increasing light intensity ($\leq 100 \text{ mW cm}^{-2}$), as can be observed in Fig. 5d, while that of DSSCs at light intensities greater than 100 mW cm^{-2} exhibits a more gradual decrease. The reduction in both J_{sc} and V_{oc} values at high operating temperatures results in decreasing PCE values at different light intensities.

On the basis of photovoltaic performance parameter measurements, one can expect to easily maintain the optimized PCE value of DSSCs with very little temperature influence at higher light intensities ($>100 \text{ mW cm}^{-2}$). However, in order to maintain the optimized PCE of DSSCs that were measured at relatively low light intensities ($\leq 100 \text{ mW cm}^{-2}$), it is necessary to either increase the light intensity using a solar concentrator or lower the operating temperature of DSSCs using a cooling system, or both. Our findings provide a better understanding of the conditions required for optimum DSSC performance.

4. Conclusions

We systematically investigated the effects of light intensity and operating temperature on the photovoltaic performance of DSSCs. Firstly, a Peltier-cell-assisted temperature control system enabled us to observe the effect of temperature on the photovoltaic properties of DSSCs. As a result, the PCE of DSSCs at the fixed 1-Sun condition significantly decreased with increasing operating temperature, which resulted in reduced liquid electrolyte viscosity that promoted ion mobility and simultaneously accelerated the charge recombination rate between photogenerated electrons and liquid iodide ions. Secondly, the use of a neutral-filter- and condenser-lens-assisted light intensity control system enabled us to observe the effect of light intensity in conjunction with operating temperature on the photovoltaic performance of DSSCs. At low light intensities ($\leq 100 \text{ mW cm}^{-2}$), the resulting PCE of DSSCs significantly decreased with increasing operating temperature. However, at high light intensities ($>100 \text{ mW cm}^{-2}$), the PCE of DSSCs was stably maintained due to the increased concentration of photogenerated electrons, which resulted in an increase in electron injection into the TiO_2 NPs and simultaneously mitigating the loss of electrons by charge recombination. In order to maintain the optimized photovoltaic performance of DSSCs in practical applications, we suggest that DSSCs can be installed in cold and sunny environments with the simultaneous use of various effective auxiliary facilities (e.g. solar concentra-

tor and cooling system) for artificially controlling the light intensity and operating temperature. We believe that our results can significantly contribute to the development of solar cells as viable alternative energy sources.

Acknowledgement

This study was supported by a 2-Year Research Grant of Pusan National University.

References

- Ahn, J.Y., Cheon, H.K., Kim, W.D., Kang, Y.J., Kim, J.M., Lee, D.W., Cho, C.Y., Hwang, Y.H., Park, H.S., Kang, J.W., Kim, S.H., 2012. *Chem. Eng. J.* 188, 216–221.
- Ahn, J.Y., Kim, J.H., Moon, K.J., Park, S.D., Kim, S.H., 2013a. *Nanoscale* 5, 6842–6850.
- Ahn, J.Y., Kim, J.H., Moon, K.J., Kim, J.H., Lee, C.S., Kim, M.Y., Kang, J.W., Kim, S.H., 2013b. *Solar Energy* 91, 41–46.
- Ahn, J.Y., Moon, K.J., Kim, J.H., Lee, S.H., Kang, J.W., Lee, H.W., Kim, S.H., 2013c. *ACS Appl. Mater. Interfaces* 6, 903–909.
- Akira, U., 2009. *Solar energy mater. Solar Cells* 93, 840–842.
- Barnes, P.R., Anderson, A.Y., Durrant, J.R., O'Regan, B.C., 2011. *Phys. Chem. Chem. Phys.* 13, 5798–5816.
- Berginc, M., Krašovec, U.O., Hočevar, M., Topič, M., 2008. *Thin Solid Films* 516, 7155–7159.
- Berginc, M., Krašovec, U.O., Jankovec, M., Topič, M., 2007. *Solar energy mater. Solar Cells* 91, 821–828.
- Calogero, G., Marco, G.D., 2008. *Solar energy mater. Solar Cells* 92, 1341–1346.
- Choi, S.C., Cho, E.N.R., Lee, S.M., Kim, Y.W., Lee, D.W., 2011. *Opt. Exp.* 19, A818–A823.
- Faustini, M., Nicole, L., Boissiere, C., Innocenzi, P., Sanchez, C., Grosso, D., 2010. *Chem. Mater.* 22, 4406–4413.
- Gonzalez-Valls, I., Yu, Y., Ballesteros, B., Oro, J., Lira-Cantu, M., 2011. *J. Power Sources* 196, 6609–6621.
- Halme, J., Saarinen, J., Lund, P., 2006. *Solar energy mater. Solar Cells* 90, 887–899.
- He, W., Chow, T.T., Ji, J., Lu, J., Pei, G., Chan, L.S., 2006. *Appl. Energy* 83, 199–210.
- Hore, S., Vetter, C., Kern, R., Smit, H., Hinsch, A., 2006. *Solar energy mater. Solar Cells* 90, 1176–1188.
- Kim, H.J., Kim, D.E., 2012. *Solar Energy* 86, 2049–2055.
- Kim, J., Kim, J., Lee, M., 2010. *Nanotechnology* 21, 345203.
- Kong, J.H., Kim, T.H., Kim, J.H., Park, J.K., Lee, D.W., Kim, S.H., Kim, J.M., 2014. *Nanoscale* 6, 1453–1461.
- Koo, H.J., Kim, Y.J., Lee, Y.H., Lee, W.I., Kim, K., Park, N.G., 2008. *Adv. Mater.* 20, 195–199.
- Lagemaat, A.J., Frank, 2001. *J. Phys. Chem. B* 105, 11194–11205.
- Lee, G.W., Kim, D., Ko, M.J., Kim, K., Park, N.G., 2010. *Solar Energy* 84, 418–425.
- Li, G.R., Wang, F., Jiang, Q.W., Gao, X.P., Shen, P.W., 2010. *Angew. Chem. Int. Ed.* 49, 3653–3656.
- Min, W.L., Jiang, B., Jiang, P., 2008. *Adv. Mater.* 20, 3914–3918.
- Mittelman, G., Kribus, A., Dayan, A., 2007. *Energy Convers. Manage.* 48, 2481–2490.
- Moon, K.J., Lee, S.W., Lee, Y.H., Kim, J.H., Ahn, J.Y., Lee, S.J., Kim, S.H., 2013. *Nanoscale Res. Lett.* 8, 283.
- Mor, G.K., Shankar, K., Paulose, M., Varghese, O.K., Grimes, C.A., 2006. *Nano Lett.* 6, 215–218.
- Muduli, S., Game, O., Dhas, V., Vijayamohan, K., Bogle, K.A., Valanoor, N., Ogale, S.B., 2012. *Solar Energy* 86, 1428–1434.
- Ocakoglu, K., Yakuphanoglu, F., Durrant, J.R., Icli, S., 2008. *Solar energy mater. Solar Cells* 92, 1047–1053.
- O'Regan, B., Durrant, J.R., 2006. *J. Phys. Chem. B* 110, 8544–8547.

- Park, Y.B., Im, H., Im, M., Choi, Y.K., 2011. *J. Mater. Chem.* 21, 633–636.
- Park, S.H., Kim, B.K., Lee, W.J., 2013. *J. Power Sources* 239, 122–127.
- Raga, S.R., Fabregat-Santiago, F., 2012. *Phys. Chem. Chem. Phys.* 15, 2328–2336.
- The National Weather Service, Solar Energy Resource Distribution Map. 2012.
- Tripagnagnostopoulos, Y., Nousia, T.H., Souliotis, M., Yianoulis, P., 2002. *Sol. Energy* 72, 217–234.
- Tripathi, B., Yadav, P., Kumar, M., 2014. *Sol. Energy* 108, 107–116.
- Zhang, Y., Wang, J., Zhao, Y., Zhai, J., Jiang, L., Song, Y., Zhu, D., 2008. *J. Mater. Chem.* 18, 2650–2652.
- Zhu, J., Hsu, C.M., Yu, Z., Fan, S., Cui, Y., 2010. *Nano Lett.* 10, 1979–1984.
- Zhu, P., Nair, A.S., Yang, S., Peng, S., Ramakrishna, S., 2011. *J. Mater. Chem.* 21, 12210–12212.